Effects of Streamlining a Bluff Body in the Laminar Vortex Shedding Regime

Ritvik Dobriyal
Earth Observatory of Singapore
School of Physical and Mathematical Sciences
Nanyang Technological University
50 Nanyang Avenue
Singapore 639798, Singapore

Maneesh Mishra
School of Mechanical and Aerospace Engineering
Nanyang Technological University
50 Nanyang Avenue
Singapore 639798, Singapore

Markus Bölander
Department of Aeronautical and Vehicle Engineering
Royal Institute of Technology
SE-100 44 Stockholm
Sweden

Martin Skote*
School of Aerospace, Transport and Manufacturing
Cranfield University
College Rd, Cranfield MK43 0AL, UK
E-mail address: M.Skote@cranfield.ac.uk

ABSTRACT

Two-dimensional flow over bluff bodies is studied in the unsteady laminar flow regime using numerical simulations. In previous investigations, lift and drag forces have been studied over different cross section shapes like circles, squares and ellipses. We aim to extend the previous research

*Address all correspondence for to this author.

by studying the variation of hydrodynamic forces as the shape of the body changes from a circular cylinder to a more streamlined or a bluffer body. The different body shapes are created by modifying the downstream circular arc of a circular cylinder into an ellipse, hence elongating or compressing the rear part of the body. The precise geometry of the body is quantified by defining a shape factor. Two distinct ranges of shape factors with fundamentally different behavior of lift and drag are identified. The geometry constituting the limit is where the rear part ellipse has a semi minor axis of half the radius of the original circle, independent of the Reynolds number. On the other hand, the vortex shedding frequency decreases linearly over the whole range of shape factors. Furthermore, the variation of the forces and frequency with Reynolds number, and how the relations vary with the shape factor are reported.

INTRODUCTION

Flow around bluff bodies over a range of Reynolds numbers gives rise to a well-known periodic flow phenomenon of vortex shedding in the wake, more familiarly known as the von Kármán vortex street [1–3]. This kind of flow has been of academic interest for years and is also relevant for many practical applications in the designing of buildings, bridges, vortex flow-meters, towers etc., as vortex shedding results in periodically varying lift and drag forces on the body. The nature and periodicity of the fluctuating forces and vortex street depends upon the Reynolds number $Re = VD/\nu$, based on the freestream velocity V, dimension of bluff body D and kinematic viscosity of fluid ν. From previous work it has been established that the flow over circular cylinders is laminar, two-dimensional (2D), and displays vortex shedding in the range of Re from approximately 50 to 170 [4–6]. At lower values of Re than this, the flow is steady and at higher values it starts to become three-dimensional [1, 7–9].

In previous studies, lift and drag forces have been studied over different cross section shapes like circles [10–15], squares [16, 17], ellipses [18–20] and half-circles [21–25]. We aim to extend the previous research by studying the variation of hydrodynamic forces and vortex shedding frequency as the shape of the body changes from a circular cylinder to a more streamlined or a more bluff body. The different body shapes are created by modifying the downstream circular arc of a circular cylinder into an ellipse.

Applications may include novel designs of heat exchangers or risers in the offshore oil-gas industry, apart from the more obvious engineering problems listed earlier. The present study points out that when shape changes are introduced in the design and optimization process, extrapolation of the forces from the original geometries are unreliable. The simulations presented here forms a guideline on which changes in the forces can be expected when streamlining a shape or transforming it into a more bluff body.

PROBLEM FORMULATION AND NUMERICAL SIMULATION

The two parameters which are varied in the present study are Re and shape factor (SF), which is defined as the ratio of length of body downstream of point of maximum thickness to half of its

maximum thickness (Fig. 1). For a circular cylinder, half of maximum thickness is the radius, while its length downstream the point of maximum thickness is also the radius. Therefore, for a circular cylinder, the SF is unity. The semi-cylinder (with the rounded section facing the flow), on the other hand, has a SF of zero according to this definition. Other bluff bodies retain the same thickness and are created by elongating or squeezing the downstream section of circular cylinder by ellipse of appropriate dimensions. For an elongated body, the downstream circular arc is replaced by an ellipse of semi major axis greater than the radius. In contrast, for a squeezed body, the downstream circular arc is replaced by an ellipse of semi minor axis lesser than the radius (Fig. 2). Accordingly, SF for the bodies in the present study is equal to the ratio of semi major or semi minor axis of ellipse to the radius of the original circle. A total of eleven bluff bodies are considered (including the circular geometry). For seven bodies, the semi minor/major axis of ellipses ranging from 0.5 to 2 in interval of 0.25 as shown in Fig. 2 in black. The remaining four bodies with SF of 0.375, 0.25, 0.125 and 0.01 are presented in red in Fig. 2. The reason for this grouping of the bodies is the different behavior of the force parameters in the respective group, and in subsequent plots the color coding is kept.

The incompressible flow is governed by the law of conservation of mass and momentum. Thus, the two-dimensional continuity and Navier-Stokes equations are solved in the present simulations. To carry out numerical simulations, a rectangular computational domain was chosen with a size of $30D \times 60D$, where D is the diameter of circular cylinder. Domain and grid size independence was ensured for all the simulations presented here. The computational domain is shown in Fig. 3, with velocity inlet (uniform parallel flow) used on the left side of domain, while the right hand side consists of zero pressure and zero velocity gradient, which allows the fluid to exit the domain. On the top and bottom symmetry boundary condition is used which allows the fluid to slip over the boundaries, while on the body no-slip condition is used.

For generating the mesh on this computational domain, it was divided into various sections as indicated in Fig. 3. In the present mesh, X = 15D, M = 0.5D. Note that the body is illustrated with an enlarged solid circle in order to clarify the grid structure near the surface. Please refer to Fig. 4 for a drawing in correct scale.

Most effort was spent on refinement of region M which is essential for capturing the boundary layer and its separation. The number of divisions on M were increased until the values for maximum lift coefficient, mean drag coefficient and Strouhal number were no longer varying at a $Re = 100$. Details are given in Tab. 1. The final number of divisions on M was determined to be 40 as further refinement did not alter the results. Furthermore, the results did not change with more refinement of grid in the outer regions.

Side O is divided into 80 control volumes, and the whole circumference of the circle is divided into 400 equally spaced segments and each side of the square containing the body has 100 divisions each (i.e, side X is divided into 50 control volumes). As mentioned above, side M (shown in red in Fig. 3) has 40 equally spaced segments making the division size 0.0125D. Side N (shown in black) has 200 segments of increasing size away from the body, with the first (smallest) division as 0.0125D to match the size of the divisions on side M.

The final developed grid is shown in Fig. 4. The meshes for other bluff bodies were generated similarly by extending the rear part of cylinder and using same dimensions for computational domain, and smallest division.

A non-dimensional time step Δt of 0.02 was found to produce accurate results by comparison with simulations with $\Delta t = 0.001$, where time is scaled by the ratio of D to V. The tolerance for residual convergence was set to 1×10^{-5}. The governing equations are discretized using the finite volume method with a second order spatial scheme and implicit time discretization, and solved using a commercially available package FLUENT.

HYDRODYNAMIC FORCES

Variables quantifying the forces and their fluctuations are lift coefficient (C_L), drag coefficient (C_D) and Strouhal number (St). The lift and drag forces on the bluff bodies vary in a sinusoidal manner with time, while their amplitudes and frequencies are dependent on Re and SF. Lift and drag coefficients per unit depth are defined as

$$C_L = \frac{F_L}{1/2\rho V^2 D}, \tag{1}$$

and

$$C_D = \frac{F_D}{1/2\rho V^2 D}, \tag{2}$$

where F_L and F_D are the lift and resistance forces of the body, respectively, and ρ is the density of the fluid.

The non-dimensional frequency of lift and drag forces is expressed by $St = fD/V$ where f is the frequency of variation of lift, while the frequency for the drag force is twice as large. We define C_{Lmax} as the maximum extreme value of C_L, while the average value of C_L is zero due to symmetry.

Re is varied from 60 to 160 in order to keep the flow in the 2D unsteady regime of vortex shedding [9, 15]. In our numerical simulations, the flow for bodies with $SF = 1.75$ and 2.0 are found to be steady for $Re = 60$ and are hence excluded from the analysis.

Lift coefficient

It is known that for a circular cylinder the maximum value of the lift coefficient (C_{Lmax}) increases with Re. In the present study, bodies with SF other than unity behave similarly. However, C_{Lmax} is dramatically affected by a change in SF. The variation of C_{Lmax} for the whole range of SF (at $Re = 100$) is shown in Fig. 5. The variation is linear for $SF \geq 0.5$. For all Re studied here it is possible to express the relation between the two variables with a linear equation of the form

$$C_{Lmax} = \frac{\mathrm{d}C_{Lmax}}{\mathrm{d}SF} \times SF + C_{Lo} \tag{3}$$

where $\frac{\mathrm{d}C_{Lmax}}{\mathrm{d}SF}$ is defined as the sensitivity of maximum coefficient of lift to SF and C_{Lo} is the intercept for the equation. The values obtained for the sensitivity and the intercept for different Re are shown in Tab. 2. From the table it can be deduced that the sensitivity of C_{Lmax} increases (in magnitude) with Re.

The C_{Lmax} for $SF \leq 0.5$ is plotted with stars in Fig. 5 and increases when lowering the SF from 0.5 to 0.375, following the previous trend. However, on further decreasing the SF, C_{Lmax} begins to fall and reaches a value of 0.41 for $SF = 0.01$ which is close to values reported by [25] and [24] for a semi-circular cylinder. The values of C_{Lmax} for $SF = 0.01$ at other Re are given in Tab. 2 and compared with the available data in the literature for a semi-circular cylinder.

Drag coefficient

Fluctuations in the drag coefficient due to vortex shedding are very weak as compared to its mean value. Therefore, only the changes in mean drag with Re and SF are considered here. The mean drag coefficient (C_{Dmean}) for a circular cylinder in the unsteady laminar flow regime was found to become nearly constant above $Re = 100$ as shown in Fig. 6. This result is consistent with the previous results of Park [15] and Rajani [8].

However, the variation of C_{Dmean} with Re for $SF > 1.0$ is the opposite from bodies with $SF < 1.0$ (see Fig. 6); decreasing for the former, while increasing for the latter. Thus, the limiting case is the circular cylinder ($SF = 1$).

Although C_{Dmean} varies little with Re for a particular body, it changes dramatically when varying SF for a particular Re as shown in Fig. 7, where results for $Re = 100$ is given. The variation of mean drag with SF for $SF \geq 0.5$ can be best described in terms of a power law of the form

$$C_{Dmean} = A \times SF^n \tag{4}$$

The agreement between Eqn. (4) with the data points obtained from the numerical simulations (circles) is shown for $Re = 100$ in Fig. 7. The values for A and n obtained for the other Reynolds numbers are given in Tab. 3, which demonstrates that the value of coefficient A remains almost constant while n falls with Re. This indicates that C_{Dmean} falls more steeply with SF at higher Re.

The bodies with $SF < 0.5$ are presented with stars in Fig. 7. The logarithmic behavior according to Eqn. (4) is clearly not valid for $SF < 0.5$. Instead, a linear relationship is revealed as seen in the inset of Fig. 7 where only the data for $SF = 0.01 - 0.5$ is shown. The linear behavior is also confirmed for other Re and the coefficients are given in Tab. 3 for the expression,

$$C_{Dmean} = \frac{\mathrm{d}C_{Dmean}}{\mathrm{d}SF} \times SF + C_{Do} \tag{5}$$

The value of the intercept C_{Do} in the expression (5) for $Re = 100$ is 1.722, which is very close to the value 1.73 reported by Farhadi et al. [23] for a semi-circular cylinder (i.e. for $SF = 0$).

The mean drag on a bluff body comprises of mean pressure drag and mean skin friction drag expressed by the coefficients C_{Dp} and C_{Dsf}, which are defined as in Eq. 2 with F_D replaced by the forces obtained by integrating the pressure difference and the wall shear stress over the surface, respectively.

A comparison of the coefficients C_{Dp} and C_{Dsf} with previous studies of a circular cylinder is shown in Fig. 8, where it can be seen that they agree well with the present results for $SF = 1$.

C_{Dsf} variation with Re remains identical for all SF, which is natural since the attached flow on the front of the cylinder is not affected by the SF. Hence, it can be concluded that the difference in mean drag (shown in Fig. 6) is due to the change in pressure drag caused by the streamlining of

the body. Bodies which are more bluff have higher pressure drag as compared to bodies which are elongated and more streamlined. Due to the contribution to C_{Dmean} by C_{Dsf} , which is independent on SF, the C_{Dp} variation with Re for the different bodies is very similar to the mean pressure in Fig. 6. However, for the pressure drag the limiting case (for which C_{Dp} is constant with varying Re) is the body with $SF = 1.25$.

Strouhal number

Classical curve fit for variation of St with Re for a circular cylinder were given by Roshko [26] and Williamson [27] and the present results agree well, see Fig. 9. Similar results were obtained for all SF varying between 0.01 and 2.0, where the St was also found to increase with Re. However, for bodies with lower SF, St was higher while it was lower for bodies with higher SF, as shown in Fig. 10. Furthermore, for all Re, the St decreases linearly with increasing SF. Similar to lift and drag, the sensitivity of St to SF was also studied. The variation of St with SF is perfectly represented by a linear relation of the form

$$St = \frac{\mathrm{d}St}{\mathrm{d}SF} \times SF + St_o \tag{6}$$

where $\mathrm{d}St/\mathrm{d}SF$ is the sensitivity of St to SF and St_o is the intercept. Values for these two variables are given in Tab. 4 for different Re, which are valid for the whole range of SF between 0.01 and 2.0. From the table it can be seen that the sensitivity of St remains almost constant with Re.

In addition, St for a semi-circular cylinder was found to be 0.188 at $Re = 100$ by [23], which exactly corresponds to the intercept in Tab. 4 for this Re. Hence, unlike the lift coefficient, the shedding frequency follows the linear behavior to the extreme case of $SF = 0$. This is evident from table 4 where close agreement exists between St_0 and St for $SF = 0.01$.

CONCLUSION

In contrast to the geometries considered previously, the present study provides a detailed description of forces acting on the bluff body and shedding frequency as the circular cylinder is elongated ($SF > 1.0$) to make it more streamlined, or squeezed ($SF < 1.0$) so that it approaches a semi-circular geometry ($SF = 0$).

Variation of C_{Lmax} (decreasing) with increasing SF was found to be linear for $SF \geq 0.5$, while a non-linear relation exists for $SF \leq 0.5$. On the other hand, the variation of C_{Dmean} (decreasing) was described by a power law for $SF \geq 0.5$, whereas a linear relation was found for $SF \leq 0.5$. Hence, both C_{Dmean} and C_{Lmax} changes behavior for $SF \leq 0.5$.

While C_{Dmean} is increasing or decreasing with Re depending on whether SF is less than or larger than unity (circular cylinder), the pressure drag coefficient behaves similarly but with the limiting case of $SF = 1.25$. The skin friction coefficient and its variation with Re remained unaffected by the SF.

The linear variation (decreasing) of St with SF could be extrapolated to the case of $SF = 0$ which corresponds to semi-circular cylinder, and the value obtained was identical to earlier simulations of this geometry. The increasing trend of St with Re remained the same for all SF and the rate of decrease of St with larger SF remained almost identical at different Re.

REFERENCES

[1] Zdravkovich, M., and Bearman, P., 1998. *Flow around circular cylinders. Volume 1: Fundamentals*. American Society of Mechanical Engineers.

[2] Schlichting, H., 1979. *Boundary layer theory*, 7th ed. McGraw-Hill.

[3] Green, S. I., 1995. *Fluid Vortices: Fluid Mechanics and Its Applications*, Vol. 30. Springer.

[4] Perry, A., Chong, M., and Lim, T., 1982. "The vortex-shedding process behind two-dimensional bluff bodies". *Journal of Fluid Mechanics,* **116**, pp. 77–90.

[5] Roshko, A., 1954. On the development of turbulent wakes from vortex streets. Tech. Rep. NACA 1191, California Institute of Technology.

[6] Bloor, M. S., 1964. "The transition to turbulence in the wake of a circular cylinder". *Journal of Fluid Mechanics,* **19**(02), pp. 290–304.

[7] Williamson, C., 1996. "Vortex dynamics in the cylinder wake". *Annual Review of Fluid Mechanics,* **28**(1), pp. 477–539.

[8] Rajani, B., Kandasamy, A., and Majumdar, S., 2009. "Numerical simulation of laminar flow past a circular cylinder". *Applied Mathematical Modelling,* **33**(3), pp. 1228–1247.

[9] Mansy, H., Yang, P.-M., and Williams, D. R., 1994. "Quantitative measurements of three-dimensional structures in the wake of a circular cylinder". *Journal of Fluid Mechanics,* **270**, pp. 277–296.

[10] Braza, M., Chasaing, P., and Ha Minh, H., 1986. "Numerical study and physical analysis of the pressure and velocity fields in the near wake of a circular cylinder". *Journal of Fluid Mechanics,* **165**(79-130), p. 41.

[11] Posdziech, O., and Grundmann, R., 2007. "A systematic approach to the numerical calculation of fundamental quantities of the two-dimensional flow over a circular cylinder". *Journal of fluids and structures,* **23**(3), pp. 479–499.

[12] Tritton, D., 1959. "Experiments on the flow past a circular cylinder at low reynolds numbers". *Journal of Fluid Mechanics,* **6**(04), pp. 547–567.

[13] Dennis, S., and Chang, G.-Z., 1970. "Numerical solutions for steady flow past a circular cylinder at reynolds numbers up to 100". *Journal of Fluid Mechanics,* **42**(3), pp. 471–489.

[14] R. Gautier, D. Biau, E. L., 2014. "A reference solution of the flow over a circular cylinder at re = 40". *Computers and Fluids,* **75**, pp. 103–111.

[15] Park, J., Kwon, K., and Choi, H., 1998. "Numerical solutions of flow past a circular cylinder at reynolds numbers up to 160". *KSME International Journal,* **12**(6), pp. 1200–1205.

[16] Sohankar, A., Norberg, C., and Davidson, L., 1998. "Low-reynolds-number flow around a square cylinder at incidence: study of blockage, onset of vortex shedding and outlet boundary condition". *International Journal for Numerical Methods in Fluids,* **26**(1), pp. 39–56.

[17] Yoon, D.-H., Yang, K.-S., and Choi, C.-B., 2010. "Flow past a square cylinder with an angle of incidence". *Physics of Fluids,* **22**, p. 043603.

[18] Mittal, R., and Balachandar, S., 1996. "Direct numerical simulation of flow past elliptic cylinders". *Journal of Computational Physics,* **124**(2), pp. 351–367.

[19] Lugt, H., and Haussling, H., 1974. "Laminar flow past an abruptly accelerated elliptic cylinder at 45 incidence". *Journal of Fluid Mechanics,* **65**(04), pp. 711–734.

[20] Kim, M.-S., and Sengupta, A., 2005. "Unsteady viscous flow over elliptic cylinders at various thickness with different reynolds numbers". *Journal of mechanical science and technology,* **19**(3), pp. 877–886.

[21] Chandra, A., and Chhabra, R., 2011. "Flow over and forced convection heat transfer in newtonian fluids from a semi-circular cylinder". *International Journal of Heat and Mass Transfer,* **54**(1–3), pp. 225 – 241.

[22] Boisaubert, N., Coutanceau, M., and Ehrmann, P., 1996. "Comparative early development of wake vortices behind a short semicircular-section cylinder in two opposite arrangements". *Journal of Fluid Mechanics,* **327**, 11, pp. 73–99.

[23] Farhadi, M., Sedighi, K., and Fattahi, E., 2010. "Effect of a splitter plate on flow over a semi-circular cylinder". *Proceedings of the Institution of Mechanical Engineers, Part G: Journal of Aerospace Engineering,* **224**(3), pp. 321–330.

[24] Bhinder, A. P. S., Sarkar, S., and Dalal, A., 2012. "Flow over and forced convection heat transfer around a semi-circular cylinder at incidence". *International Journal of Heat and Mass Transfer,* **55**(19–20), pp. 5171 – 5184.

[25] Chatterjee, D., Mondal, B., and Halder, P., 2013. "Unsteady forced convection heat transfer over a semicircular cylinder at low reynolds numbers". *Numerical Heat Transfer, Part A: Applications,* **63**(6), pp. 411–429.

[26] Ahlborn, B., Seto, M. L., and Noack, B. R., 2002. "On drag, strouhal number and vortex-street structure". *Fluid dynamics research,* **30**(6), pp. 379–399.

[27] Williamson, C., 1989. "Oblique and parallel modes of vortex shedding in the wake of a circular cylinder at low reynolds numbers". *Journal of Fluid Mechanics,* **206**, pp. 579–627.

LIST OF FIGURES

LIST OF TABLES

FIGURES

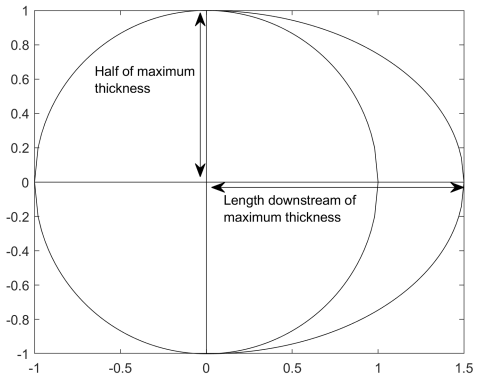

Fig. 1. Diagram showing the body with $SF = 1.5$, with inscribed circular geometry indicating half of the maximum thickness and the length of body downstream the point of maximum thickness. The flow is from left to right.

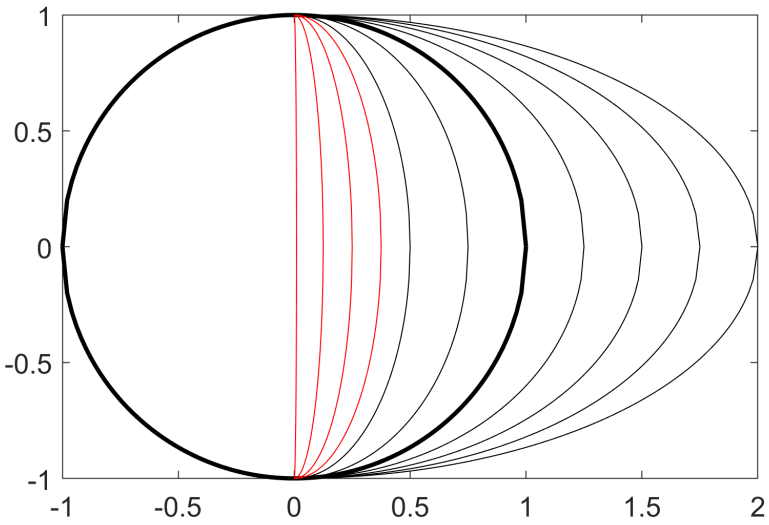

Fig. 2. The bluff body shapes used in the study. Bodies with $SF \geq 0.5$ are in black while those with $SF < 0.5$ are shown in red color.

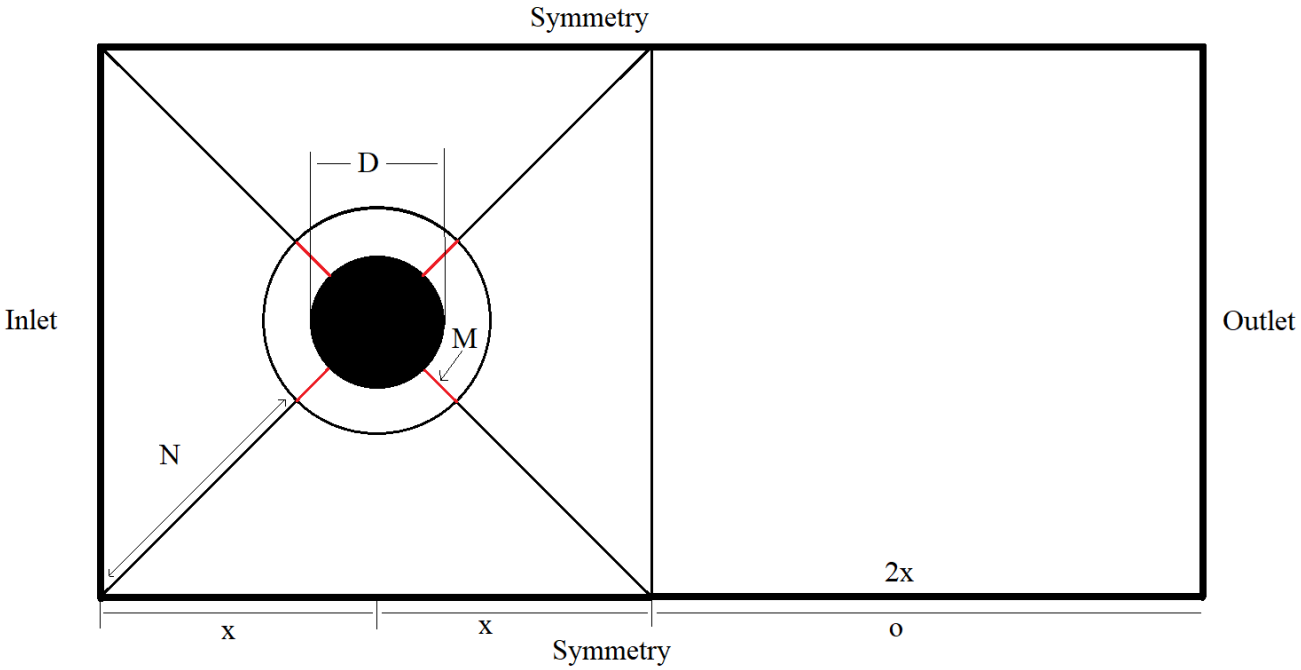

Fig. 3. Computational domain with the different mesh regions. Cylinder and the surrounding area is presented in larger scale for clarity.

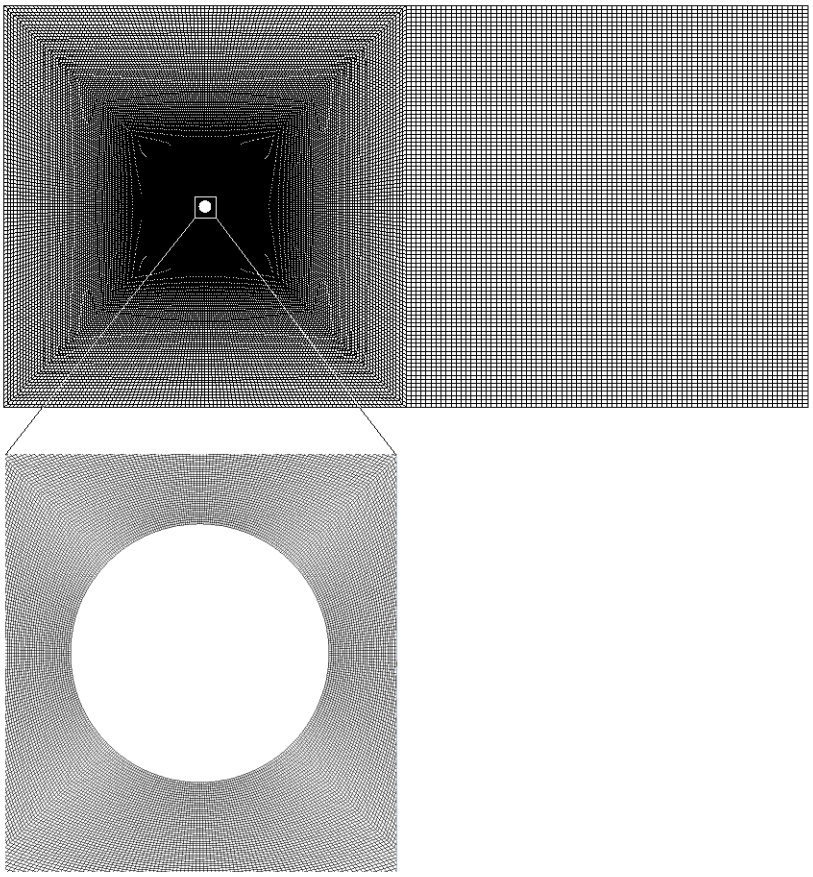

Fig. 4. Structured mesh for carrying out numerical simulations. The flow is from left to right.

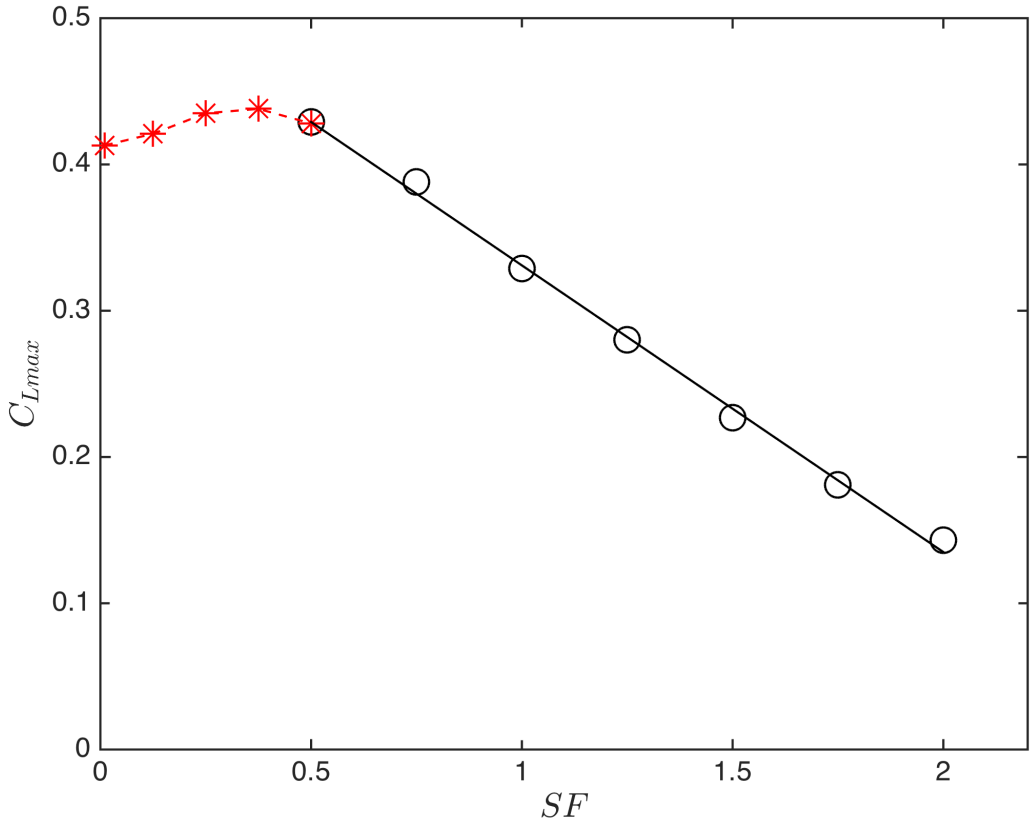

Fig. 5. Variation of C_{Lmax} with SF at $Re = 100$ together with expression (3) as the solid line.

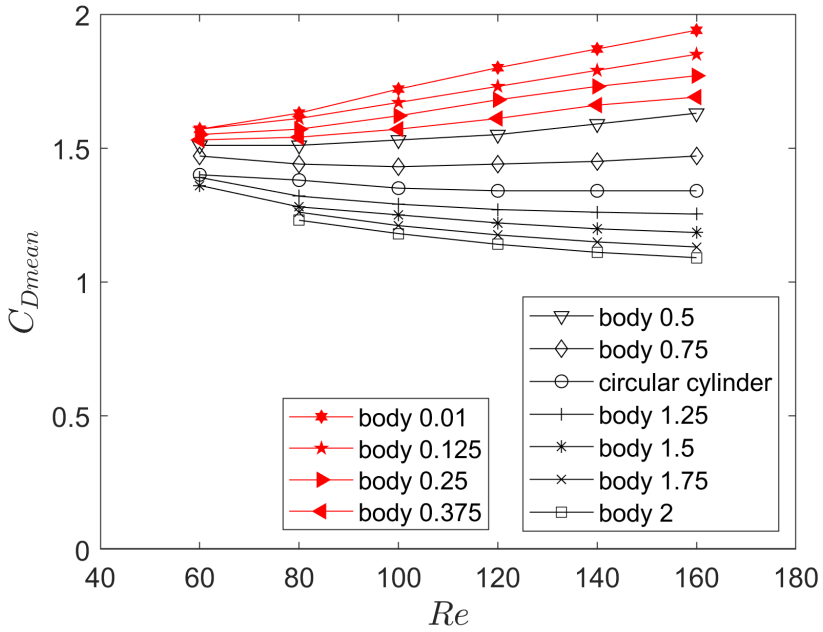

Fig. 6. Variation of C_{Dmean} with Re for different body shapes. The numbers in the legend refer to the SF. The circular cylinder corresponds to $SF = 1.0$.

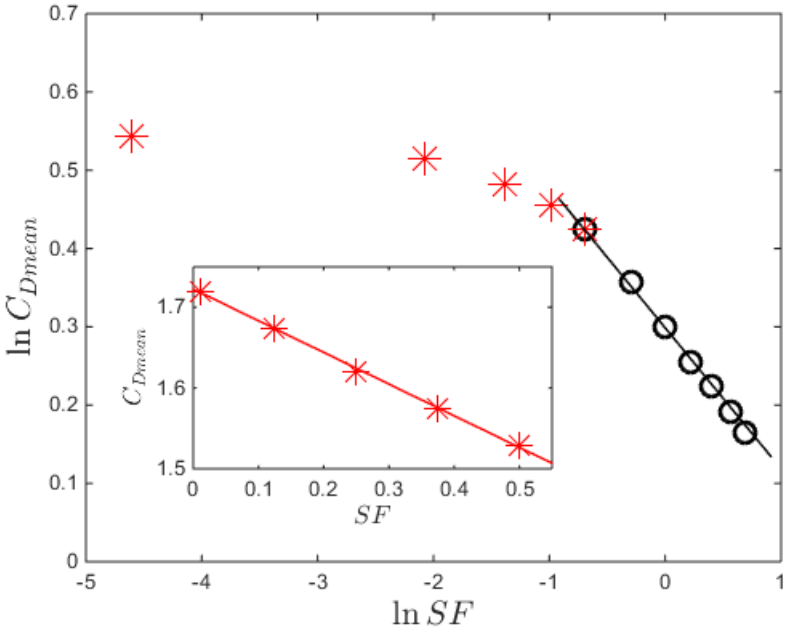

Fig. 7. Variation of C_{Dmean} with SF at $Re = 100$ in logarithmic scale. Rings symbolize the original simulation and stars the additional simulation. The solid line is Eqn. (4) with $A = 1.347$ and $n = -0.18$. The inset illustrates the linear relation of the additional data, with the solid line representing Eqn. (5) with intercept $C_{Do} = 1.722$ and slope $\frac{\mathrm{d}C_{Dmean}}{\mathrm{d}SF} = -0.392$.

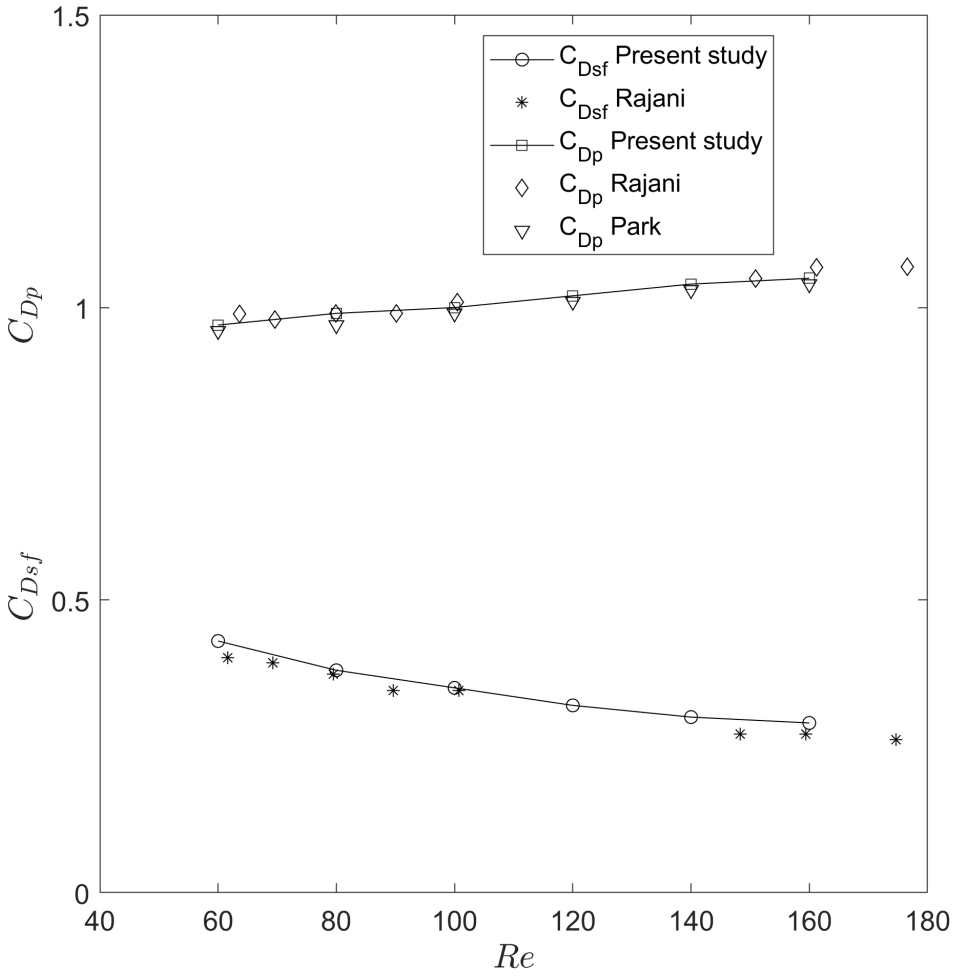

Fig. 8. Comparison of pressure drag (C_{Dp}) and skin friction drag (C_{Dsf}) in present study for circular cylinder with previous results reported by Park [15] and Rajani [8].

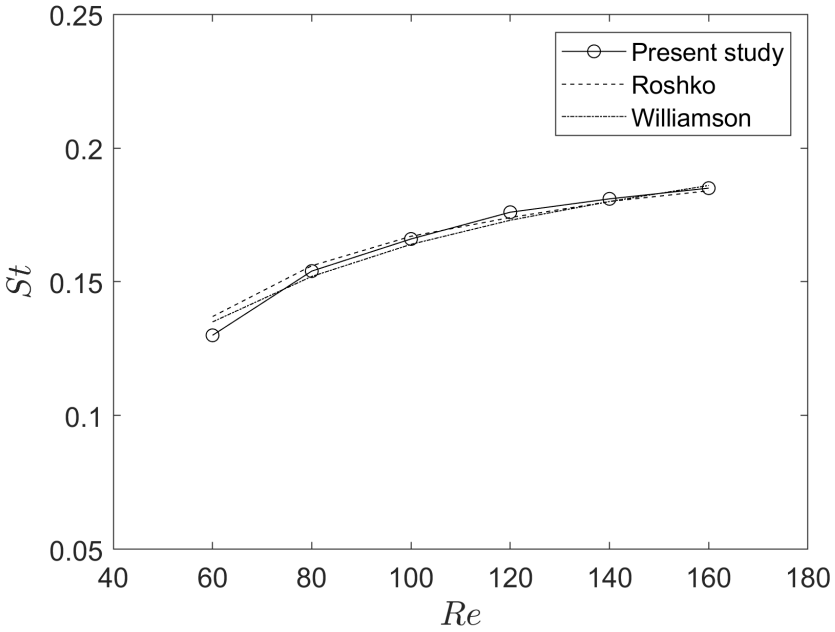

Fig. 9. Comparison of St in the present study for a circular cylinder with classical curve fit from Roshko [26] and Williamson [27].

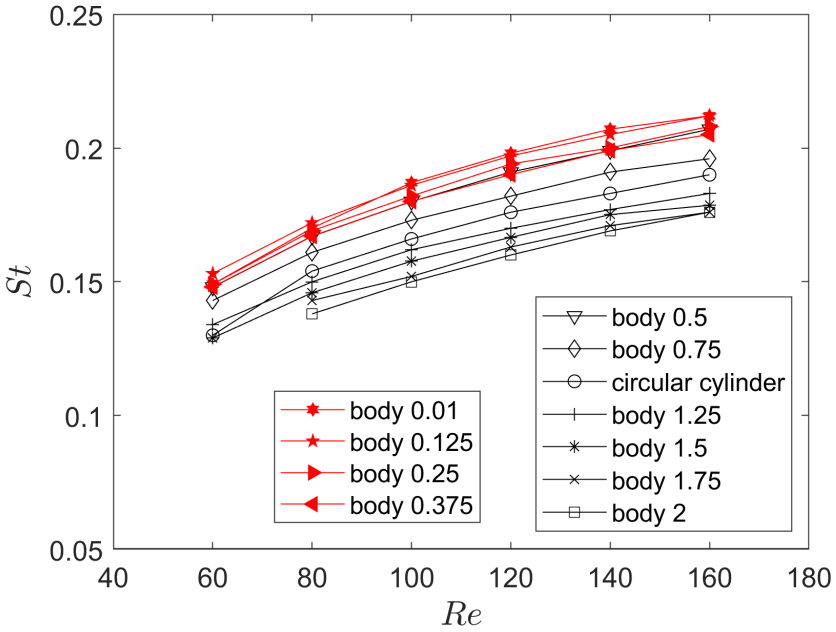

Fig. 10. St variation with Re for different body shapes.

TABLES

Table 1. Grid variation study

Divisions on M	Maximum lift coefficient	Mean drag coefficient	St
20	0.311	1.45	0.165
30	0.324	1.4	0.166
40	0.329	1.35	0.166
50	0.329	1.35	0.166

Table 2. Coefficients of Eqn. (3) at different Re

Re	$\mathrm{d}C_{Lmax}/\mathrm{d}SF$	C_{Lo}	C_{Lmax} $(SF = 0.01)$	C_{Lmax} [24]
60	-0.114	0.242	0.15	
80	-0.149	0.388	0.29	0.30
100	-0.196	0.527	0.41	0.42
120	-0.248	0.663	0.51	0.52
140	-0.302	0.792	0.59	
160	-0.346	0.908	0.65	0.64 $(Re = 150)$

Table 3. Coefficients for Eqn. (4), valid for $SF \geq 0.5$ and Eqn. (5), valid for $SF \leq 0.5$

Re	A	n	C_{Do}	$\frac{\mathrm{d}C_{Dmean}}{\mathrm{d}SF}$
60	1.415	-0.09	1.584	-0.142
80	1.367	-0.15	1.641	-0.263
100	1.347	-0.18	1.722	-0.392
120	1.336	-0.22	1.807	-0.507
140	1.334	-0.26	1.880	-0.590
160	1.337	-0.29	1.937	-0.630

Table 4. Coefficients for Eqn. (6)

Re	$\mathrm{d}St/\mathrm{d}SF$	St_0	St for $SF = 0.01$
60	-0.018	0.157	0.150
80	-0.018	0.174	0.171
100	-0.020	0.188	0.187
120	-0.020	0.197	0.198
140	-0.019	0.205	0.207
160	-0.020	0.212	0.212